ACS Biomaterials SCIENCE & ENGINEERING

Article

pubs.acs.org/journal/abseba

In Vivo Expansion of Melanoma-Specific T Cells Using Microneedle Arrays Coated with Immune-Polyelectrolyte Multilayers

Qin Zeng,[†] Joshua M. Gammon,[†] Lisa H. Tostanoski,[†] Yu-Chieh Chiu,[†] and Christopher M. Jewell*[,†,‡,§]

[†]Fischell Department of Bioengineering, University of Maryland, College Park, 8228 Paint Branch Drive, 2212 Jeong H. Kim Building, College Park, Maryland 20742, United States

[‡]Department of Microbiology and Immunology, University of Maryland Medical School, 685 West Baltimore Street, HSF-I Suite 380, Baltimore, Maryland 21201, United States

[§]Marlene and Stewart Greenebaum Cancer Center, 22 S. Greene Street, Suite N9E17, Baltimore, Maryland 21201, United States

Supporting Information

ABSTRACT: Microneedles (MNs) are micron-scale polymeric or metallic structures that offer distinct advantages for vaccines by efficiently targeting skin-resident immune cells, eliminating injection-associated pain, and improving patient compliance. These advantages, along with recent studies showing therapeutic benefits achieved using traditional intradermal injections in human cancer patients, suggest MN delivery might enhance cancer vaccines and immunotherapies. We recently developed a new class of polyelectrolyte multilayers based on the self-assembly of model peptide antigens and molecular toll-like receptor agonists (TLRa) into ultrathin, conformal coatings. Here, we reasoned that these immune polyelectrolyte multilayers (iPEMs) might be a useful platform for assembling cancer vaccine components on MN arrays for intradermal delivery from these substrates. Using conserved human melanoma antigens and a potent TLRa vaccine adjuvant, CpG, we show that iPEMs can be assembled on MNs in an automated fashion. These films, prepared with up to 128 layers, are approximately 200 nm thick but provide cancer vaccine cargo loading >225 $\mu g/cm^2$. In cell culture, iPEM cargo released from MNs is internalized by primary dendritic cells, promotes activation of these cells, and expands T cells during coculture. In mice, application of iPEM-coated MNs results in the codelivery of tumor antigen and CpG through the skin, expanding tumor-specific T cells during initial MN applications and resulting in larger memory recall responses during a subsequent booster MN application. This study support MNs coated with PEMs built from tumor vaccine components as a well-defined, modular system for generating tumor-specific immune responses, enabling new approaches that can be explored in combination with checkpoint blockade or other combination cancer therapies.

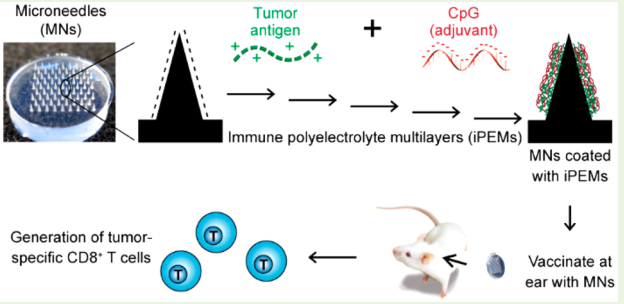

KEYWORDS: *microneedle, cancer, vaccine, polyelectrolyte multilayer, self-assembly, immunology*

INTRODUCTION

The skin is an important component of the immune system as a barrier but also as a network that is rich in antigen presenting cells (APCs) able to survey the periphery for foreign molecules.[1] These cells are immunologically important in infectious disease, in tolerance, and in cancer. Dendritic cells (DCs), Langerhans cells, and other APCs traffic these antigens to lymph nodes (LNs), presenting peptide fragments to lymphocytes that drive adaptive immunity after activation and migration from LNs or other immunological tissues. This high concentration of APCs, along with ease-of-access, has made the skin one of the most effective vaccination routes, intradermal-injection (*i.d.*), in particular.[2−5] As with all traditional needle-based injections, intradermal injections create medical sharps, require training for effective administration, and cause pain, of particular relevance since a high percentage of vaccine recipients are children. Further, the vaccines themselves often require refrigeration, a cold chain that is problematic for developing countries. Not surprisingly, immense interest has thus developed in microneedles (MNs), polymeric or metallic structures that offer features to overcome all of the challenges above.[6−8] MNs improve patient compliance by eliminating medical sharps and injection-associated pain, while also often providing thermal stability and dose-sparing for vaccines or drugs loaded on or within MNs.[9,10] These devices also allow consistent delivery to specific target tissues, such as within the skin (i.e., intradermally), or as another example, the supra-choroidal space at the back of the eye.[11]

Most MN approaches fall into one of four modalities: solid microneedles for prepenetration of the skin, coated microneedles, hollow microneedles, and dissolvable microneedles.[6−8]

Special Issue: Biomaterials for Immunoengineering

Received: July 22, 2016
Accepted: September 1, 2016
Published: September 1, 2016

DOI: 10.1021/acsbiomaterials.6b00414
ACS Biomater. Sci. Eng. 2017, 3, 195−205

Scheme 1. Approach for Assembling Immune Polyelectrolyte Multilayers on Microneedle Arrays to Enhance Cancer Vaccination

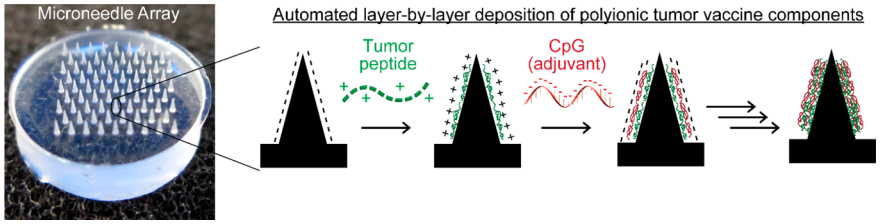

The design constraints (e.g., dosing needs, kinetics, and cargo stability) for a specific application drive the choice of these strategies, but all of these options are attractive because they offer rapid vaccine administration through the stratum corneum, an important immunological barrier in the skin. Thus, nearly all MN vaccines strategies have been aimed at prophylactic vaccination against infection, influenza,[12−14] HIV,[15−17] and hepatitis,[18,19] to name a few. However, there are tremendous opportunities to apply these technologies to therapeutic vaccines and immunotherapies in the context of cancer, in part for the reasons above, such as APC targeting, but also owing to some unique considerations. For example, several recent studies in human patients and animal models suggest that intradermal injection improves antitumor responses during melanoma and prostate cancer vaccination.[20−22]

Recently, a few studies have begun demonstrating the unique potential of MNs for cancer vaccination. Some of these approaches have generated antitumor immunity in preclinical models using microneedles to penetrate the skin prior to topical administration of tumor antigens encoded in plasmids or isolated from tumor cell cultures.[23,24] Thus far, none of these strategies has incorporated tumor antigens on or within MNs for cancer vaccination. However, some recent work has utilized dissolvable polymeric microneedles loaded with polymeric nanoparticles encapsulating model antigens (ovalbumin, OVA) to target Langerhans cells and provide protection during challenge with melanoma cells expressing OVA.[25,26] Several other recent reports have used MNs to support the delivery of cancer immunotherapies including cytokines,[27] chemotherapeutics,[28] and cutting-edge checkpoint inhibitors.[29]

One important coating technology that has been applied to microneedles for prophylactic vaccination but not yet for cancer vaccination is polyelectrolyte multilayers (PEMs).[17,30−34] PEMs are assembled by electrostatic interactions and offer unique features such as the ability to juxtapose multiple cargos with tunable control over the relative loading and ultrathin coatings that allow conformal films to be assembled on the fine geometries of MN arrays.[35] We recently reported a new type of PEM assembled entirely from immune signals, immune PEMs (iPEMs).[36−38] These films are composed of antigens modified with cationic amino acid residues and nucleic acid−based toll-like receptor (TLR) agonists that serve both as adjuvants and as negatively charged structural components of the films. In contrast to other PEMs used in drug and vaccine delivery, iPEMs eliminate all other polymers or film components. This feature simplifies vaccine design through modular assembly of immune signals while preserving attractive features such as codelivery and tunable control over the absolute and relative loading of film components. In particular for cancer vaccination, our studies reveal that iPEMs codeliver the vaccine components used to build the films, enhancing APC costimulation and the function of T cells expanded by these populations. Thus, we hypothesized iPEMs would be an attractive platform to coat microneedles to create the first tumor-antigen specific vaccine delivered using microneedles.

Here, we show that iPEMs can be assembled on poly(L-lactide) (PLLA) MNs using a conserved human melanoma antigen, tyrosinase-related protein 2 (Trp2),[39] and CpG oligonucleotide, a potent TLR9 agonist that has been intensely studied as a vaccine adjuvant (Scheme 1).[40] Trp2 peptide modified with a cationic nona-arginine (R_9) domain (Trp2*) supports stable assembly with CpG using an automated LbL process to deposit up to 128 layers on PLLA MN arrays with linear control over the loading of both tumor antigen and the CpG adjuvant. Cargo released from MNs *in situ* and incubated with primary immune cells promotes uptake and activation of APCs, triggering functional responses in Trp2-specific T cells during coculture. In mice, MNs coated with Trp2*/CpG iPEMs deliver both signals to ear immunization sites, resulting in expansion of tumor-specific T cells during priming MN immunizations and more potent memory recall responses during booster MN applications. This work could enable a new approach to cancer vaccination based on combining MNs to deliver tumor vaccine components self-assembled at high density into PEMs.

MATERIALS AND METHODS

Materials. $Trp2_{180−188}$ (SVYDFFVWL), Trp2* (SVYDFFVWL-RRRRRRRRR), and $SIIN_{257−264}$ (SIINFEKL) peptide from OVA protein were synthesized by Genscript with >98% purity, with or without a FITC label on the N-terminus. TLR9 agonist CpG oligonucleotide (5′T*C*C*A*T*G*A*C*G*T*T*C*C*T*-G*A*C*G*T*T 3′) and a nonimmunostimulatory control oligonucleotide (CTRL, 5-T*C*C*T*G*A*G*C*T*T*G*A*A*G*T-3) were synthesized by IDT with a phosphorothioate backbone. Label-IT nucleic acid labeling kits (Cy5) were purchased from Mirus Bio LLC. Poly(L-lactide) (PLLA) and poly(sodium 4-styrenesulfonate) (SPS) were purchased from Sigma-Aldrich. Poly(ethylenimine) (PEI, MW 25 k) was purchased from Polysciences, Inc. A Sylgard silicone-elastomer kit was obtained from Dow Corning.

Animals and Care. C57BL/6J mice (female, 6−8 weeks) were obtained from The Jackson Laboratory. Breeding pairs of transgenic mice displaying T cell receptors specific for Trp2 were a gift from Dr. Giorgio Trinchieri (National Cancer Institute, National Institutes of Health). All animal care and experiments were carried out using protocols approved and overseen by the University of Maryland IACUC committee in compliance with local, state, and federal guidelines.

Assembly and Characterization of iPEMs on Planar Substrates. All bilayers were assembled using a DR3 dipping robot (Riegler & Kirstein GmbH). First, PEI/SPS baselayers were built on a planar substrate for 10 bilayers to provide a uniform charged surface. Silicon wafers (Silicon Inc.) and quartz slides (VWR) were cut into 5 mm × 25 mm substrates using a diamond dicing saw (model 1006, Micro Automation). Substrates were cleaned via sequential rinsing in acetone, ethanol, methanol, and water, dried under filtered air, and charged with an oxygen plasma deposition system (Jupiter III, March).

DOI: 10.1021/acsbiomaterials.6b00414
ACS Biomater. Sci. Eng. 2017, 3, 195−205

The prepared substrates were then coated with the PEI/SPS precursor layers by alternative dipping into a filtered PEI solution (20 mM polymer; 50 mM NaCl; 5 mM HCl in water) for 5 min and SPS (20 mM polymer; 50 mM NaCl in water) for 5 min, separated by two sequential 1 min rinsing steps in deionized water. Following a total of 10 cycles, the precursor-coated substrates were coated with iPEMs using the same dipping and wash times but using Trp2* as the polycation (0.5 mg/mL, 0.2 M sodium acetate) and CpG as the polyanion (0.5 mg/mL, 0.2 M sodium acetate). In some studies, fluorescently labeled peptide (FITC-Trp2*) and CpG (Cy5-CpG) were used to facilitate tracking during experiments. After depositing the desired number of layers, 2, 4, 8, 16, or 32 bilayers, chips were dried under filtered air. Film thickness was measured during deposition at defined intervals using a Stokes Ellipsometer (Gaertner Scientific) to allow monitoring of film growth. For each reading, the thickness at five locations on at least three separate substrates was recorded and averaged. In studies designed to quantify relative cargo loading as a function of the number of layers, iPEMs were assembled on quartz chips, and UV−visible spectrophotometry was used to record the absorbance values from 200 to 600 nm. Wavelengths of 260 and 488 nm were used to identify the loading of CpG and FITC-Trp2*, respectively. For release assays, planar substrates coated with FITC-Trp2*/CpG bilayers were incubated in PBS buffer adjusted with 2 M NaCl and to different pH values: 4, 6, 8, 10, and 12. After 24 h, the substrates were removed, and the remaining film thickness was measured by ellipsometery (silicon substrates), while the amount of cargo released into solution was determined using a microBCA assay (Thermo Scientific) for FITC-Trp2* and by UV−visible spectrophotometry for CpG. The pH of each solution was adjusted back to 7.4 using HCl or NaOH solution prior to all measurements.

MN Fabrication. MNs arrays were prepared as previously described.[16] Briefly, poly(dimethylsiloxane) (PDMS) molds using a Sylgard 184 silicon elastomer kit (Dow-Corning) were prepared using a Clark-MXR-CPA-2010 (VaxDesign). PLLA was melted through a phase transition in the molds under vacuum (−25 in. Hg, 200 °C, 40 min), then cooled to −20 °C for least 30 min before separating the cast PLLA microneedles from the PDMS mold. MN morphology was characterized by scanning electron microscopy (SEM) using a JEOL 6700F FEG-SEM and confocal laser scanning microscope (CLSM) using a Leica SP5X instrument.

Assembly and Characterization of iPEMs on MNs. Trp2*/CpG bilayers were coated onto MN arrays using a protocol similar to the procedure described above, but PEI/SPS precursor layers were not used. To assemble iPEMs on MNs, the MN arrays were sequentially exposed for 5 min each to Trp2* (1 mg/mL, 0.2 M sodium acetate buffer), with or without a FITC label, and CpG (1 mg/mL, 0.2 M sodium acetate), with or without a Cy5 label. These deposition steps were separated by two sequential 1 min rinsing steps in deionized water, with fresh rinse solutions used for each cycle. Assembly on MNs was automated using a DR3 dipping robot programmed to repeat the bilayer deposition a desired number of times, up to 64 bilayers (128 layers). For quantification, the needles on MN arrays were removed and then incubated in DMSO at room temperature (RT) for 24 h. The loading amounts of CpG and Trp2 were calculated by UV−visible spectrophotometry and microBCA assay, respectively, then reported on an area basis. Release products were characterized using a similar approach described above for planar substrates. Coated MN arrays were incubated in the indicated solutions, then the components released into the solutions were characterized using dynamic light scatting (DLS) for size and electrophoretic mobility for surface charge using a Zetasizer Nano ZS90 (Marvern). The concentrations of each component in similarly prepared solutions were determined by fluorescence and absorbance as described above.

Cell Internalization Studies. Uptake of iPEM cargo released from MNs by DCs was characterized by flow cytometry (FACS CantoII, BD Bioscience) and confocal microscopy (Leica SP5X). Cargo was released from MNs by incubation of iPEM-coated MN arrays in PBS solutions adjusted to pH 10 for 24 h. After release, the incubation solutions were collected and adjusted to pH 7.4. DCs were isolated from the spleens of naïve C57BL/6J mice (The Jackson Laboratory) using a $CD11c^+$ magnetic isolation system (Miltenyi Biotec). For flow cytometry studies, $CD11^+$ splenic DCs were seeded in 96-well plates at a concentration of 1.0×10^5 cells per well in RPMI 1640 media (Lonza), supplemented with 10% fetal bovine serum (FBS, Corning), 2 mM L-glutamine (Gibco), 55 μM β-mercaptoethanol (Sigma-Aldrich) 1× nonessential amino acids (Fisher Scientific), 10 mM HEPES (Fisher Scientific), 100 units/mL of penicillin, and 100 μg/mL of streptomycin (Gibco). 2-Fold serial dilutions were then prepared from the MN cargo release solutions beginning with the undiluted solution, which contained 5 μg/mL Trp2* and 4.1 μg/mL CpG. Twenty microliters of PBS (control) or of each cargo release solution was then added to the wells, in triplicate, containing the DCs in 180 μL of media. Cells were then cultured for 20 h. After incubation, cells were washed twice by centrifugation and resuspended in FACS buffer (PBS in 1% BSA). The washed cells were finally resuspended in 4′,6-diamidino-2-phenylindole (DAPI, 0.1% in PBS with 1% BSA) to measure viability (i.e., $DAPI^-$ cells) by flow cytometry. Cells positive for FITC and the Cy5 signal were gated among live cells compared with negative controls and single color staining controls.

Cell internalization was confirmed directly using confocal microscopy by incubating 5×10^6 DCs (prepared as described above in 1 mL media) with 20 μL of MN cargo release solution. The final concentration of released cargo in the medium was 10.0 μg/mL Trp2* and 8.2 μg/mL CpG. Four hours later, the cells were gently washed three times with PBS, then fixed with 4% paraformaldehyde for 15 min at 37 °C, and washed twice with PBS. Cell membranes were stained with tetramethyl rhodamine labeled wheat germ agglutinin conjugate (5 μg/mL in PBS; Invitrogen) at RT for 10 min protected from light. After three additional washes in PBS, cells were resuspended in Hoescht stain (4 μg/mL) to visualize nuclei, and the signals of Hoescht (nuclei), FITC (peptide), rhodamine (cell membrane), and Cy5 (CpG) were imaged by confocal microscopy.

Dendritic Cell Activation Studies. $CD11c^+$ DCs were obtained as described above and plated (1×10^5 cells/well) in complete RPMI 1640 media (Lonza). Samples, added to wells in triplicate, included PBS, lipopolysaccharide (LPS, 1 μg/mL), CpG (5 μg/mL), CTRL oligonucleotide (5 μg/mL), SIIN peptide (5 μg/mL), or iPEM cargo released from MNs coated with (Trp2*/CpG, 5 μg/mL for Trp2* and 4.1 μg/mL CpG, repectively). The release solutions from these MNs corresponded to final doses in the medium of 5.0 μg/mL Trp2* and 4.1 μg/mL CpG. Cultures were incubated for 24 h, then collected by centrifugation (800 g, 5 min), washed twice in FACS buffer, and blocked with anti-CD16/CD32 (BD Biosciences). The cells were finally stained for 20 min at RT using monoclonal antibody against the surface activation markers CD40, CD80, and CD86 (BD Bioscience). After staining, cells were washed twice and resuspended in FACS buffer containing DAPI for analysis by flow cytometry.

T Cell Proliferation Studies. $CD11c^+$ DCs from naïve C57BL/6J mice were isolated and treated as described above for DC activation studies. After 48 h of culture, naïve $CD8^+$ T cells were isolated by magnetic separation (StemCell Technologies) from the spleens of Trp2 transgenic mice. T cells from these mice display T cell receptors specific for Trp2. Isolated $CD8^+$ T cells were stained with carboxyfluorescein succinimidyl ester (CSFE, 5 μM) and washed 3 times, then 2.5×10^5 labeled T cells were added to the DC cultures. After another 60 h of coculture, cells were washed and blocked, as described above. Cells were then stained with anti-CD8 (BD Biosciences) for 20 min at RT, washed, and resuspended in DAPI for analysis by flow cytometry.

ELISA Assays. Supernatants from cocultures of splenic DCs and transgenic $CD8^+$ T cells were quantified by sandwich ELISA according to the manufacturer's protocols for the secretion of IFN-γ, IL-6, and IL-1β (BD Biosciences).

Application of MNs for *in Vivo* Histology and Dosing Studies. To administer MN arrays to mice, animals were anesthetized under isoflurane. The ear was then rinsed in sterile PBS and gently flattened against clean glass slides. MN arrays were then applied to one ear for 15 min under a constant mass of 0.45 kg. For trypan blue studies, uncoated MN arrays were applied, mice were sacrificed, the

DOI: 10.1021/acsbiomaterials.6b00414
ACS Biomater. Sci. Eng. 2017, 3, 195−205

ears were removed, and then 4% trypan blue dye was applied by incubation with the applied ear for 5 min. To confirm iPEM cargo delivery into skin, MNs coated with (FITC-Trp2*/Cy5-CpG)$_X$ iPEMs were applied to naïve mice for 15 min, then the arrays were removed and the mice were sacrificed. The treated portion of the skin was isolated and fixed in 4% paraformaldehyde for 10 min at RT protected from light. After three washes in PBS, the skin was observed using confocal microscopy to visualize each cargo signal. To quantify how much of the iPEM cargo was delivered to the ear from the MN array, the MNs used for treatment were dissolved in DMSO for 24 h after the treatment, then the amount of FITC-Trp2* and CpG in the DMSO solution were quantified as described above. The amount delivered to the ear was calculated by subtracting the value measured after treatment from measurements of the amount of cargo on identical MNs not applied to animals.

***In Vivo* Vaccination Studies Using iPEM-Coated MN Arrays.** C57Bl/6 mice (N = 6/group) were immunized with PBS or coated MNs on day 0 in the right ear and boosted on day 15 by application of a second MN array to the left ear. Blood was then collected by the submandibular route on days 0, 7, 14, 21, and 28. Blood samples were treated with 1 mL of ACK lysing buffer (Life Technologies) to remove red blood cells, collected by centrifugation (800 g, 5 min.), washed in FACS buffer, and collected. Each cell sample were then blocked with anti-CD16/32 for 10 min at RT, followed by staining with the MHC I Trp2 tetramer (APC-conjugated, MBL International Corp.) for 30 min at RT. Cells were subsequently surface-stained by incubation with anti-CD8a (FITC, BD bioscience) for 20 min at RT, washed twice, and suspended in FACS buffer containing DAPI for analysis by flow cytometry.

Statistical Analysis. Student's t tests were used in the comparison of two groups. One-way ANOVA with a Dunnet post-test was used to compare three or more groups. In all cases, analyses were carried out with Graphpad Prism (version 6.02). Error bars in all panels represent the mean ± SEM, and p values ≤0.05 were considered significant. Levels of significance were defined as * $p < 0.05$; ** $p < 0.01$; *** $p < 0.001$; and **** $p < 0.0001$.

RESULTS

iPEMs Allow Tunable Assembly of Cancer Vaccine Components on Planar Substrates. We first used planar substrates to evaluate the formation, loading, and stability of iPEMs built from Trp2* and CpG on the precursor layers (PL). Ellipsometry performed on silicon substrates during assembly revealed increasing thickness that grew linearly (R^2 = 0.99) at a rate of 4.6 nm per bilayer, reaching a thickness of 193.0 nm after depositing 32 bilayers of iPEMs (Figure 1A). Similarly, loading on quartz substrates revealed linear control over cargo loading for both Trp2* (Figure 1B and Figure S1; R^2 = 0.99) and CpG (Figure 1B and Figure S1; R^2 = 0.97). Next, we assessed the release behavior of iPEMs by incubating coated substrates in buffer solution at the indicated pH values (Figure 1C,D). After 24 h, release from iPEMs was pH-dependent, as indicated by both the extent of decrease in film thickness (Figure 1C) and the amount of cargo released into solution (Figure 1D). These studies revealed release of up to 23.2 ± 1.87 μg/cm^2 for Trp2* and 21.9 ± 0.32 μg/cm^2 of CpG for substrates coated with (Trp2*/CpG)$_{32}$ iPEMs. This general approach was then adapted to deposit Trp2*/CpG iPEMs on MNs for subsequent use in cell and animal studies.

iPEMs Allow Automated and Tunable Assembly of Trp2* and CpG on MN Arrays. MN arrays were fabricated from PLLA using PDMS molds to form arrays displaying a total of 77 needles, each with a diameter of 250 μm at the base and a height of 650 μm (Figure 2A–C). Next, fluorescently labeled Trp2* (FITC) and CpG (Cy5) were deposited on the MN arrays using a programmable robotic dipping system to

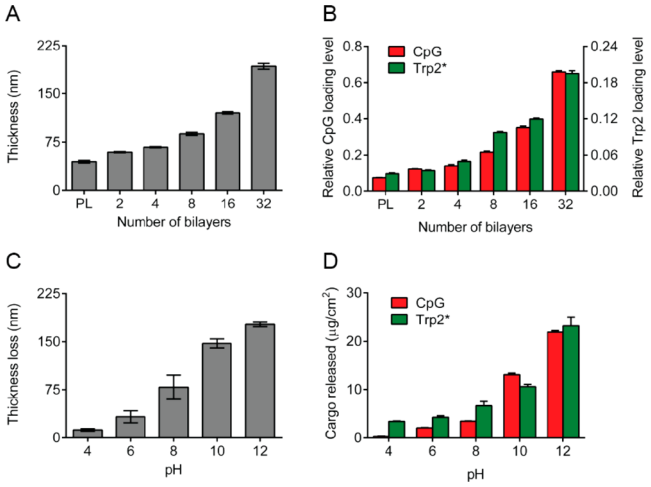

Figure 1. PEM films assembled from Trp2* and CpG can be deposited on planar substrates. (A) Thickness of iPEM films exhibiting linear growth on silicon substrates as a function of the number of layers deposited. (B) Relative loading of Trp2* peptide antigen and CpG adjuvant on quartz substrates using FITC-labeled Trp2* and CpG. (C) Decrease in film thickness on coated silicon substrates after incubation in buffer at the indicated pH conditions. (D) Quantification of cargo release from iPEMs using absorbance (CpG, 260 nm) and protein determination (Trp2*).

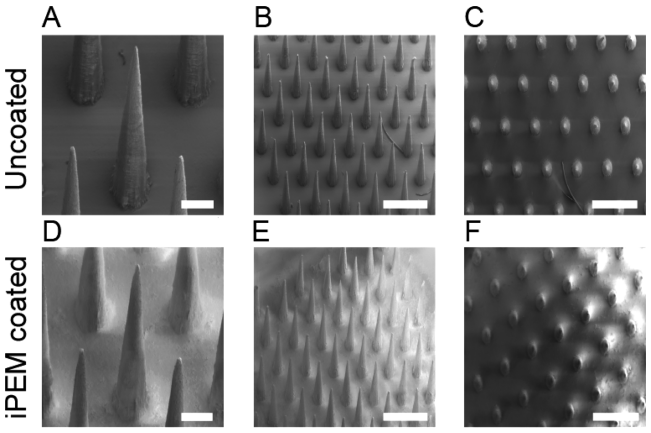

Figure 2. iPEMs composed of 64 bilayers (128 layers) of Trp2* and CpG assembled on MN arrays by robotic deposition exhibit a uniform, conformal morphology. (A–C) SEM images of uncoated MN arrays and (D–F) images of iPEM coated MNs arrays. Scale bars for A and D = 200 μm; scale bars for B, C, E, and F = 1 mm.

automate the LbL process. This LbL approach led to uniform, conformal coating on MNs even after the deposition of 64 bilayers (128 layers) (Figure 2D–F). Fluorescence microscopy of the fluorescent iPEM components assembled on the MNs revealed clear colocalization of the Trp2* and CpG signals on the surface of the individual MNs (Figure 3A). To assess film growth on MN arrays, arrays were dried after deposition of 4, 16, 32, and 64 bilayers (128 layers), then the spatial distribution of the fluorescent signal was visualized using confocal microscopy. These measurements revealed Trp2* and CpG signal intensities that were a function of the number of layers deposited (Figure 3B), colocalized, and well-defined in a given z-plane (Figure 3C), and localized to the changing circumference of MNs along the entire height (Figure 3D). Signal intensity analysis from data analogous to the representative samples shown in Figure 3B,C indicated a near-linear

DOI: 10.1021/acsbiomaterials.6b00414
ACS Biomater. Sci. Eng. 2017, 3, 195–205

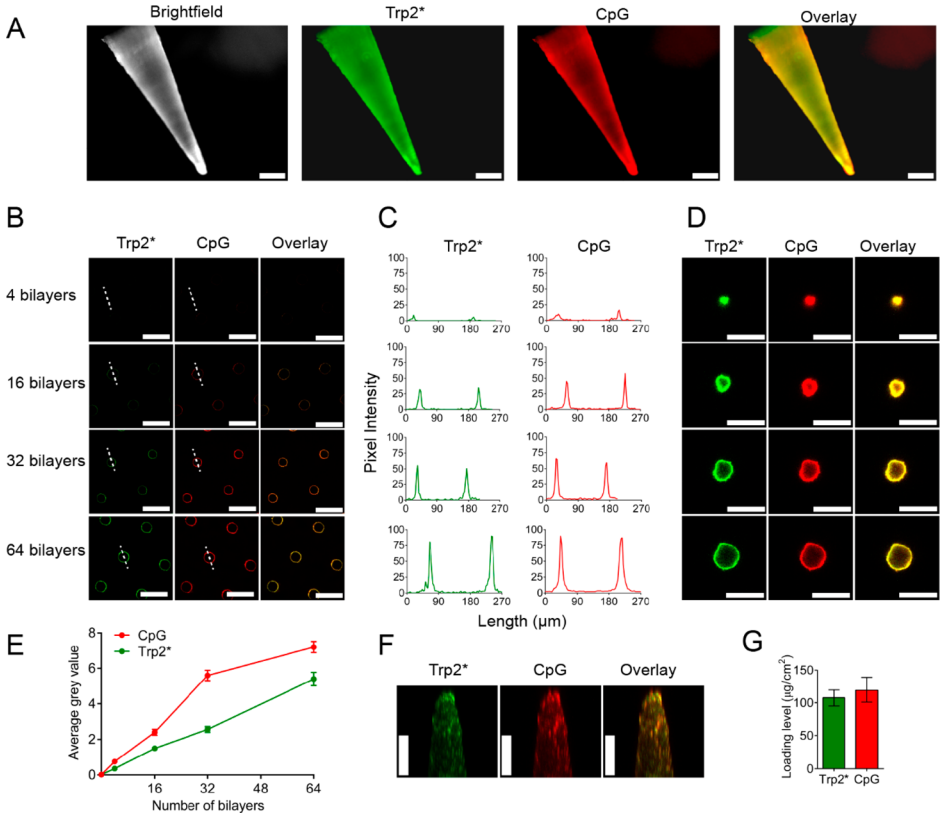

Figure 3. iPEM layers are deposited with tunable control over dose during the LbL assembly of $(Trp2^*/CpG)_{64}$. (A) Image of individual MNs visualized by florescence microscopy (Scale bar = 100 μm). (B) Confocal microscopy images demonstrating increasing signal intensity from Trp2* and CpG after 4, 16, 32, and 64 bilayers (Scale bar = 500 μm). (C) Pixel intensity traces across the corresponding dashed line in each panel in B. (D) Confocal microscopy z-stack images of MNs coated with $(Trp2^*/CpG)_{64}$ at different z positions (Scale bar = 100 μm). (E) quantification of MFI of iPEM signals from individual MNs in panel B. (F) 3D projection of MN tips from Z-stack demonstrating colocalization (yellow) of Trp2* (green) and CpG (red) along the length of the MNs (Scale bar = 50 μm). (G) Loading levels of Trp2* and CpG on MNs on a per area basis.

relationship between the number of layers deposited and fluorescent signal for Trp2* (R^2 = 0.99) and CpG (R^2 = 0.93) (Figure 3E). This was reflected by the continuous coating shown in a 3D projection from image stacks collected along the height of MNs coated with $(Trp2^*/CpG)_{64}$ iPEMs (Figure 3F). Direct measurements of the loading of each signal on MNs indicated 120.0 ± 12.7 $\mu g/cm^2$ for Trp2* and 107.8 ± 18.9 $\mu g/cm^2$ of CpG for MNs coated with 64 bilayers of Trp2*/CpG iPEMs (Figure 3G). Together, these data indicate that clinically relevant cancer vaccine components can be self-assembled into PEMs on MNs with tunable control over the loading of both Trp2* and CpG.

iPEM Cargo Released from MNs Is Internalized by DCs and Drives DC Activation. We next examined the interactions of cancer vaccine cargo released from MNs with splenic DCs. In these studies, FITC-Trp2* Cy5-CpG coated on MNs were released from the arrays in an analogous manner to Figure 1, then the size and surface charge of the released components were measured by DLS and zeta potential analysis, respectively. These studies revealed that the released cargos assembled into nanosized complexes exhibiting near-neutral charge (Figure S2). Next, the amount of cargo in each released solution was quantified (Figure 4A) and used to treat DCs isolated from spleens of mice. Following incubation, confocal microscopy confirmed the signal for both Trp2* (green signal) and CpG (red signal) in DCs (Figure 4B), while flow cytometry revealed that a significant fraction of DCs took up Trp2 and CpG in a dose dependent manner (Figure 4C). A

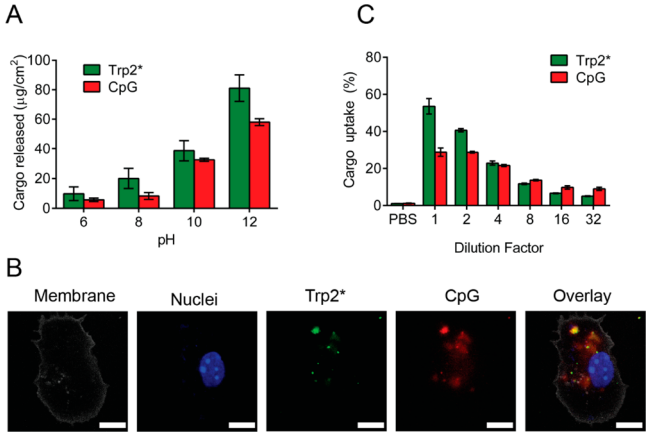

Figure 4. iPEM cancer vaccine components released from MNs coated with $(Trp2^*/CpG)_{64}$ are cointernalized by primary DCs. (A) Quantification of the release levels of each iPEM component as a function of pH used to disrupt the films. (B) Confocal microscopy images of DCs incubated for 4 h with iPEM components released from MNs demonstrate colocalization of both components in the cells (white, cell membrane; blue, nuclei; green, Trp2*; red, CpG; scale bar = 10 μm). (C) Frequency of primary DCs internalizing each iPEM component after incubation for 20 h with the cargo released from the MNs.

significant fraction of these cells were also positive for both signals, indicating codelivery. To gain insight into the

DOI: 10.1021/acsbiomaterials.6b00414
ACS Biomater. Sci. Eng. 2017, 3, 195−205

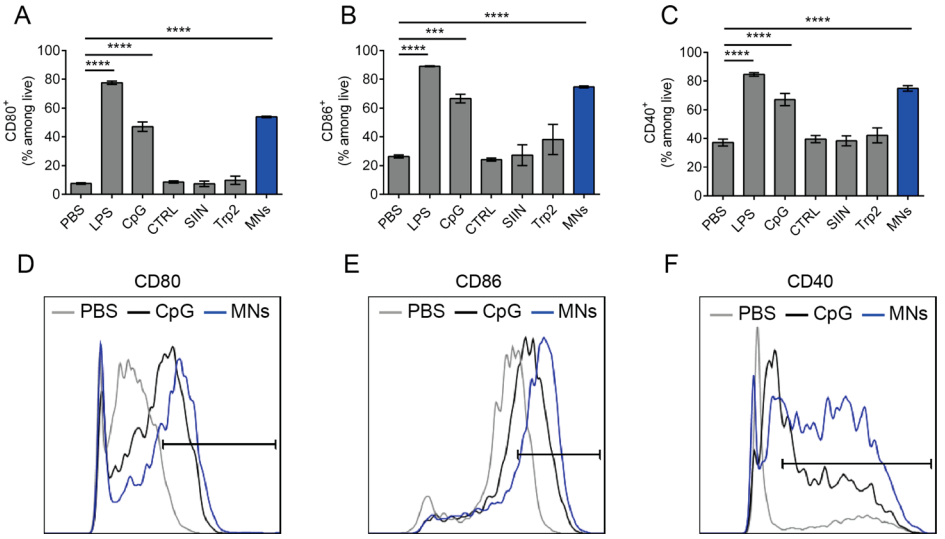

Figure 5. iPEM components released from MNs activate primary DCs. Frequency of DCs expressing costimulatory markers: (A) CD80, (B) CD86, and (C) CD40 after incubation with cargo release solutions for 24 h. Representative flow cytometry histograms showing traces for (D) CD80, (E) CD86, and (F) CD40, corresponding to panels A, B, and C, respectively.

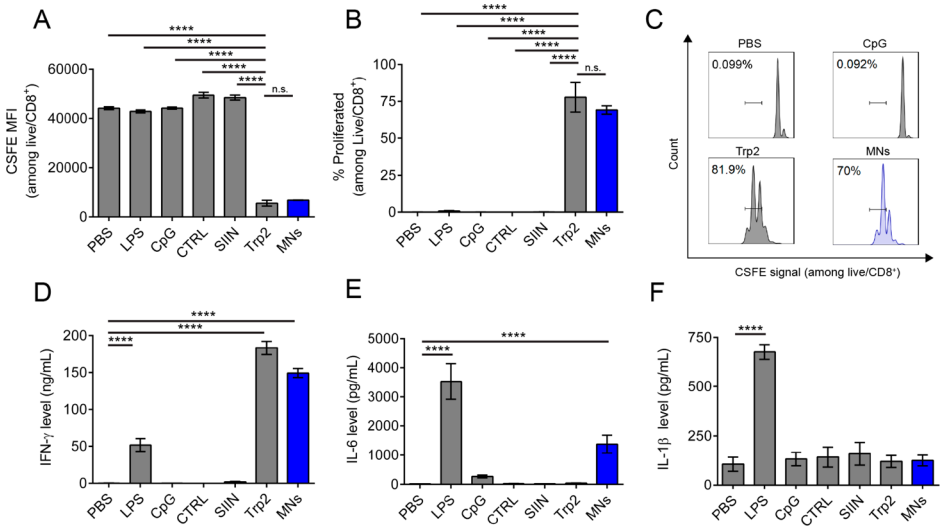

Figure 6. Increased DCs activation after incubation with released MN cargo drives proliferation of Trp2-specific transgenic CD8$^+$ T cells and effector cytokine secretion during coculture. (A) MFI of CFSE and (B) frequency of the CD8$^+$ T cells as measured by flow cytometry. (C) Representative flow cytometry histograms showing the gating scheme and frequency of T cell proliferation. (D) IFN-γ, (E) IL-6, and (F) IL-1β concentrations in supernatants from the cocultures in A, B, and C measured by ELISA. Controls are vehicle (PBS), positive control (Trp2), negative controls (CpG, LPS), and irrelevant antigen control (SIIN).

components released into solution during these studies, we incubated iPEM-coated MNs in PBS or PBS with 10% FBS (v/v) for 36 h. The released components exhibited sizes of approximately 50 nm in both buffers, while the addition of serum shifted the surface charge toward neutral values (Figure S3). With respect to cargo release, 24.2% of Trp2* and 16.4% of CpG were released in PBS, while 26.9% of Trp2* and 84.8% of CpG were released in serum containing media over this interval (Figure S3). Together, these data demonstrate that iPEMs assembled from tumor antigens and TLR agonists on MNs are released in a manner that can be efficiently internalized by primary DCs.

Next, we incubated DCs with iPEM release solutions as described above and used flow cytometry to test if uptake of iPEM components drives DC surface activation and costimulatory markers. In these experiments, DCs treated with cargo released from MN arrays exhibited high levels of CD80 (Figure 5A,D), CD86 (Figure 5B,E), and CD40 (Figure 5C,F) expression, readings that were comparable to those measured in cells treated with free LPS, a potent TLR4 agonist (Figure 5). These values were also similar to those of free CpG, which was at a similar dose to the amount of CpG in the MN release solutions (Figure 5). As expected, treatment of cells with a nonimmunostimulatory oligonucleotide (CTRL), SIIN control peptide, or Trp2* alone did not result in any significant activation relative to DCs treated with PBS (Figure 5). Analysis of mean fluorescent intensity values indicated similar results (Figure S4). Thus, assembly of iPEMs on MNs does not impact the ability of adjuvants (i.e., CpG) to activate DCs.

DCs Treated with Cargo Released from MNs Activate Trp2-Specific T Cells in Coculture. To investigate if DCs process and present Trp2 with the appropriate costimulatory

DOI: 10.1021/acsbiomaterials.6b00414
ACS Biomater. Sci. Eng. 2017, 3, 195−205

ligands needed to activate Trp2-reactive T cells, we set up a coculture system in which DCs were first cultured with MN release solutions for 48 h. These cells were then cocultured with $CD8^+$ T cells isolated from transgenic mice. In these mice, T cells display T cell receptors that recognize Trp2 peptide when displayed by APCs in the MHC I antigen presentation complex. Consequently, Trp2-reactive T cells encountering the display of this peptide−MHC complex, along with the correct costimulatory ligands on APCs, proliferate and secrete inflammatory signaling molecules (e.g., cytokines). Our studies with this coculture system revealed strong and selective proliferation in cultures treated with the MN release solutions, as indicated by the greatly reduced signal of a fluorescent tracer (CSFE) as dye is diluted during successive generations of cell proliferation. In contrast, DCs treated with adjuvant alone (LPS, CpG), nonimmunostimulatory oligonucleotide (CTRL), irrelevant peptide antigen (SIIN), or PBS did not cause T cell proliferation (Figure 6A). These control results were indicated by the high CSFE intensity measured in these samples since the cells did not divide to dilute the dye (Figure 6A). Similar findings were also reflected in the analysis of frequency data (Figure 6B) evaluated using the gates shown in Figure 6C. The results of this study demonstrate that the selectivity of Trp2 incorporated in iPEMs and released from MNs is not altered by these processes.

We next measured inflammatory and effector cytokine levels in the supernatants of coculture samples to investigate whether the cargo from MNs expand T cells that then exhibit functional characteristics (i.e., cytokine secretion). LPS-treatment resulted in high levels of pro-immune cytokines secreted by DCs (i.e., IL-6 and IL-1β), while only a modest level of a key T cell effector cytokine, IFN-γ, was observed (Figure 6D−F). In contrast, cultures treated with MN release solutions induced high levels of IFN-γ that were comparable to the levels observed in positive control cultures treated with free Trp2, the peptide recognized by the transgenic T cells (Figure 6E). The levels of IL-6 associated with MN cargo treatment were modest, while IL-1β secretion was not observed. The latter is a key component in the NALP3 inflammasome innate signaling cascade.[41] Thus, cargo released from MNs expands T cells that generate high levels of effector cytokines associated with antigen-specific immune response, rather than less-specific inflammatory reactions (e.g., inflammasome activation).

MNs Codeliver iPEMs to Skin *in Vivo*. Building on our *in vitro* results, we next applied uncoated or iPEM-coated MN arrays to the ears of mice for a period of 5 min. Staining ears with trypan blue after application of uncoated MN arrays revealed a clear penetration into the epidermis and a pattern characteristic of the MN arrangement on the arrays used in the study (Figure 7A). Similarly, confocal microscopy revealed colocalization of both iPEM components (i.e., FITC-Trp2*, green; Cy5-CpG, red) following application of MN arrays coated with $(Trp2^*/CpG)_{64}$ iPEMs (Figure 7B). Quantification of the delivered dose showed the delivery of 28.9 ± 6.4 $\mu g/cm^2$ for Trp2* (dose = 5.77 μg) and 23.6 ± 6.5 $\mu g/cm^2$ for CpG (dose = 4.84 μg) using a single array coated with $(Trp2^*/CpG)_{64}$ iPEMs (Figure 7C). These result indicate the successful codelivery of iPEM components from MNs to the skin without need for other PEM components.

Immunization with $(Trp2^*/CpG)_{64}$ iPEMs on MNs Expands Tumor-Specific T Cells. We last investigated the ability of iPEM-coated MNs to expand tumor-specific $CD8^+$ T cells in naïve mice. In these studies, mice were primed with

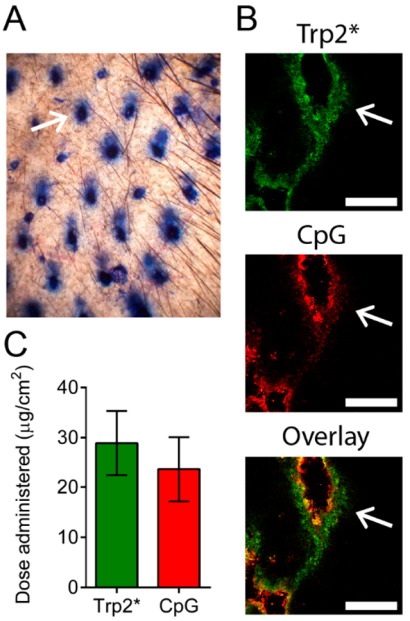

Figure 7. iPEM-coated MNs penetrate the skin and codeliver Trp2* and CpG into the skin. (A) True color image of a representative mouse ear after the application of MNs and staining with trypan blue. The arrow indicates a single penetration point. (B) Confocal microscopy images of treated skin showing the codelivery of each iPEM component (green, Trp2*; red, CpG) to an individual penetration site (arrows) after the application of MNs coated with $(Trp2^*/CpG)_{64}$ (Scale bar = 200 μm). (C) Doses of Trp2* and CpG administered to mouse skin after the application of coated MNs.

iPEM-coated MN arrays on day 0 by application to the right ear for 15 min, then boosted on day 15 using a second iPEM-coated array applied to the left ear for 15 min. Staining of peripheral blood with the MHC I Trp2 tetramer was performed weekly. After 7 days, mice immunized with MNs exhibited a slight, but statistically significant increase in the frequency of Trp2-specific $CD8^+$ T cell relative to mice treated with PBS (Figure 8A). These populations were still evident at week 2, though the statistical significance was not observed relative to the control group at this point (Figure 8A). One week after the booster injection on day 15 (i.e., day 21), a significantly higher frequency and more tightly distributed group of values were observed, while by week 4, the frequency of Trp2-specific $CD8^+$ T cell reached the highest value of the experiment (Figure 8B), with frequencies greater than 2.0% (Figure 8C). These results demonstrate that MNs coated with iPEMs generate tumor-specific T cell response and further that boosting leads to recall responses with a greater magnitude of response compared with that of the priming MN application.

DISCUSSION

Microneedles offer many advantages for prophylactic vaccination, including elimination of medical sharps and injection-associated pain, improved patient compliance, and better cargo stability. Importantly, the immunological features of skin, a high concentration of APCs, for example, and recent studies in human melanoma and prostate cancer patients highlight the potential of leveraging intradermal delivery for improving cancer immunotherapy.[20−22] Some of the unique ways intradermal delivery might be harnessed include local delivery to common skin cancers such as melanoma, as well as more-broadly applicable concepts such as using intradermal delivery

DOI: 10.1021/acsbiomaterials.6b00414
ACS Biomater. Sci. Eng. 2017, 3, 195−205

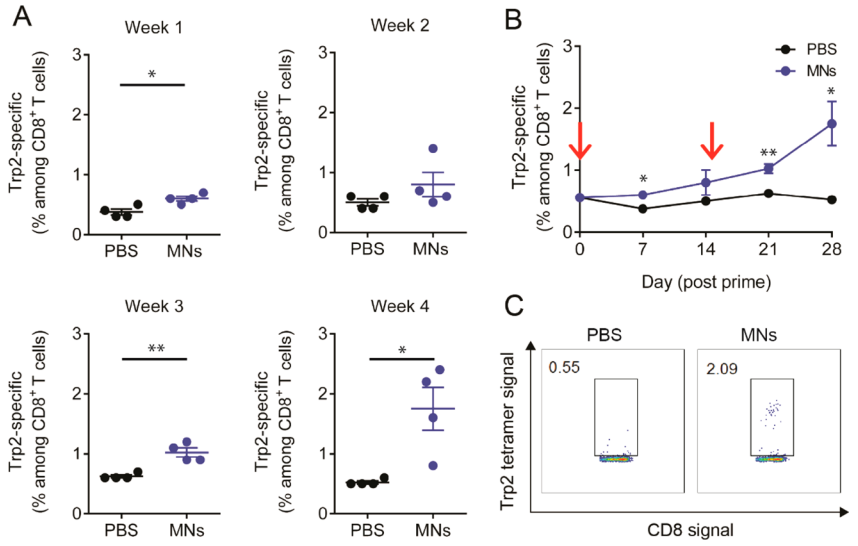

Figure 8. Cancer vaccination of mice with iPEM coated MNs promotes melanoma-specific $CD8^+$ T cells. Mice were primed at day 0 and boosted at day 15 with MNs coated with $(Trp2^*/CpG)_{64}$. (A) Frequency of Trp2 specific $CD8^+$ T cells in peripheral blood was quantified by tetramer staining weekly during priming and boosting with MNs. (B) Development of Trp2-specific $CD8^+$ T cell response over 28 days. Arrows indicated prime and booster MN applications. (C) Representative flow cytometry scatter plots demonstrating the development of a clear population of $CD8^+$ T cells specific for the Trp2 epitope as measured by the MHC I Trp2 tetramer on day 28 post prime.

to strongly activate large subsets of skin-resident immune cells already sampling but perhaps not activated against existing and neo-tumor antigens that often develop during cancer.[42] MNs, as demonstrated by the first few examples recently reported using these technologies in the context of cancer,[23−29] clearly have great potential. As discussed in the Introduction, some studies have focused on the delivery of chemotherapeutics,[28] pro-immune cytokines,[27] or signals to unleash immune functions that tumors often suppress.[29] Within the sphere of cancer vaccines, several studies have explored coating MNs with model antigens (e.g., OVA),[25,26] while a few examples have used uncoated MNs to prepenetrate the skin, then topically applied cancer vaccine components to the skin.[23,24] Our approach is distinguished from past studies because this is the first time tumor antigens have been incorporated on or within MNs. The molecules we chose are significant because Trp2 is a conserved antigen in many human cancers,[39,43,44] while CpG is a potent TLR9 agonist already being studied in human therapies.[40] Thus, we reasoned that juxtaposing Trp2 and CpG at high concentrations in iPEMs would create a simple, modular approach for MN-based cancer vaccination. This approach is also unique because of the simple set of vaccine components, eliminating synthetic polymers and polyelectrolytes, carrier components, or excipients used in all previously reported MN delivery examples.

From a materials perspective, we made several interesting discoveries in building and assessing iPEMs. First, coating of MNs with iPEMs, like traditional PEMs, allowed tunable and linear control over the loading of both the tumor antigen and the TLR agonist. One of the unique features of PEM is the stepwise and conformal nature of assembly. We exploited this idea to automate the assembly of iPEMs and observed that MNs coated in this manner were conformal even after the deposition of 128 layers (Figure 2). Positive trypan-blue signal, a dye that stains permeable cells, confirmed penetration of the skin following MN application (Figure 7). Excitingly, iPEM coated MNs were effective in expanding tumor-specific T cells in mice (Figure 8), effects that were concurrent with our observation of the colocalization of both Trp2* and CpG within the skin at the MN administration sites (Figure 7). The delivered dose in these studies was 5.77 μg for Trp2* and 4.84 μg for CpG, approximately 24% and 22% of total amount of each component loaded on the MN arrays. This is not surprising, as we did not integrate an explicit release mechanism into our assemblies in this proof-of-concept work. However, many possibilities exist for incorporating releasable technology into MNs. For PEMs in particular, strategies for releasable multilayers or incorporated cargos have included ultrasound,[45] magnetic fields,[46] laser irradiation,[47] chemical cues,[48] and integration of enzyme-sensitive polymers.[46,49] Much work has also been carried out on degradable polymers as components of PEMs to control release and delivery kinetics;[50,51] this is another promising strategy to further enhance our approach. However, the strong *in vivo* T cell responses associated with delivering only 20−25% of the iPEM dose demonstrate the potential of this strategy, along with the possibility of simply adding more layers, for tumor vaccination.

In our cell culture studies, we confirmed that iPEMs maintain the function and selectivity of the components used to build these assemblies. DCs treated with iPEMs built from CpG and Trp2*, for example, expanded transgenic T cells specific for Trp2. In our past studies with model antigens coated on colloidal templates,[36] appending cationic R_9 to these antigens was required to support PEM growth. However, R_9 is also a cell-penetrating peptide (CPP).[52,53] This and similar molecules have been used for a range of applications, such as improving cellular transport of proteins conjugated to nanoparticles.[53−55] Thus, R_9 might also contribute to the uptake or colocalization features we observed during cell cultures studies (Figure 4) or to improve interactions with skin-resident immune cells during *in vivo* immunization using iPEM-coated MN arrays. Future intracellular trafficking studies to assess the mechanisms of uptake and sequestration of these signals in immune cells will provide insight into if and how this component impacts immunogenicity.

DOI: 10.1021/acsbiomaterials.6b00414
ACS Biomater. Sci. Eng. 2017, 3, 195−205

Our cell culture studies also provided some insight into some of the immunological populations that iPEMs target. We observed that all iPEM and control samples containing Trp2 peptide caused significant proliferation, whereas the cytokine profiles between groups differed significantly (Figure 6). IFN-γ secretion was most dependent on the presence of Trp2 since this cytokine is produced by T cells upon activation (i.e., proliferation), which only occurred in Trp2-containing samples. Modest levels were observed in the LPS, one of the strongest TLR agonists. In contrast, IL-6 was observed to varying degrees whenever a TLR agonist was present, even when the antigen was absent. This is also consistent, as IL-6 plays an important role in innate immunity and is secreted by APCs.[56] Perhaps most interestingly, IL-1β, a key component of the inflammasome,[57] was not observed with iPEMs released from MNs. This is in contrast to several recent papers demonstrating that poly(lactide-*co*-glyoclide), polystyrene, and other common biomaterial carriers activate nonspecific inflammatory pathways (e.g., inflammasomes) as a result of intrinsic immunogenic features.[58−61] Thus, iPEMs improve vaccine definition by simplifying the number of vaccine and carrier components.

Microneedles themselves also offer a number of useful features, including the elimination of biomedical sharps and improved cargo stability that can facilitate scale-up. For traditional prophylactic vaccination, improved compliance owing to reduced pain and ease of application are also important benefits. However, these latter points may be less important in the context of immunotherapy and therapeutic vaccination where recipients are patients already dealing with significant illness and more invasive treatments such as surgical resection and chemotherapy.

With respect to adaptive responses, our *in vivo* studies demonstrate strong expansion of tumor specific $CD8^+$ T cells. These cytotoxic T lymphocytes are an important component of effective antitumor responses able to target and destroy cancer cells. We also showed that boosting of mice results in a significantly larger recall response that suggests the generation of immunological memory. However, an important next step will be to test the functional capacity of these cells during tumor challenge. In particular, these studies will assess if the expanded T cells confer anti-tumor immunity and if these enhancements are efficacious during early or late-stage treatments of mice challenged with melanoma or other preclinical models. Current clinical strategies being explored for cancer vaccination focused on combination therapies, such as those employing cancer vaccination to provide tumor-specific immune responses while also administering checkpoint inhibitors that release pro-immune inflammatory processes that tumors co-opt and suppress.[62] Thus, conducting challenge studies in isolation during cancer vaccination as a monotherapy is less attractive since even candidate vaccines that potently expand tumor-specific cells often fail to be curative because these cells are suppressed by the tumors.[63,64] Recent studies with MNs for delivering immunotherapies, including checkpoint inhibitors, thus set the stage for combining vaccination and cotherapies in a way that mimics some of the most-promising approaches being explored in human trials.[27,29]

CONCLUSIONS

In this study, we demonstrate the potential of using MN arrays to codeliver clinically relevant tumor peptides with human vaccine adjuvants. This system simplifies vaccine design by eliminating polymeric and excipient components, while maintaining useful features of biomaterials such as codelivery. Further, iPEMs can be assembled in a stepwise, automated manner to control cargo loading while maintaining the immunological specificity of the vaccine components. In mice, these assemblies expand tumor-specific $CD8^+$ T cells during priming injections and promote memory recall responses during boosting. The findings reported here could contribute to a new, more rational design of MN-enabled cancer vaccine platforms.

ASSOCIATED CONTENT

Supporting Information

The Supporting Information is available free of charge on the ACS Publications website at DOI: 10.1021/acsbiomaterials.6b00414.

Absorbance spectra of each iPEM component during deposition; size, zeta potential, and cargo loading measurements of cargo release from coated MNs; and MFI measurements for DC activation studies (PDF)

AUTHOR INFORMATION

Corresponding Author

*Phone: 301-405-9628. Fax: 301-405-9953. E-mail: cmjewell@umd.edu. Web: jewell.umd.edu.

Notes

The authors declare no competing financial interest.

ACKNOWLEDGMENTS

We acknowledge A. Beaven and the University of Maryland Imaging Core Facility for assistance in confocal microscopy. This work was supported in part by NSF CAREER Award # 1351688 and the University of Maryland Division of Research (Tier 1). J.M.G. is a grantee of the Pediatric Oncology Student Training award from Alex's Lemonade Stand Foundation. Y.C.C. is a trainee on NIH Grant # T32 CA154274. L.H.T. is a fellow supported by the NSF Graduate Research Fellowship Program Grant # DGE1322106. C.M.J. is a Damon Runyon-Rachleff Innovator supported by the Damon Runyon Foundation (# DRR3415), and a Young Investigator of the Alliance for Cancer Gene Therapy (# 15051543) and the Melanoma Research Alliance (# 348963).

REFERENCES

(1) Nestle, F. O.; Di Meglio, P.; Qin, J. Z.; Nickoloff, B. J. Skin immune sentinels in health and disease. *Nat. Rev. Immunol.* **2009**, *9*, 679−691.

(2) Kenney, R. T.; Frech, S. A.; Muenz, L. R.; Villar, C. P.; Glenn, G. M. Dose sparing with intradermal injection of influenza vaccine. *N. Engl. J. Med.* **2004**, *351*, 2295−2301.

(3) Whitaker, J. A.; Rouphael, N. G.; Edupuganti, S.; Lai, L.; Mulligan, M. J. Strategies to increase responsiveness to hepatitis B vaccination in adults with HIV-1. *Lancet Infect. Dis.* **2012**, *12*, 966−976.

(4) Madhusudana, S. N.; Mani, R. S. Intradermal vaccination for rabies prophylaxis: conceptualization, evolution, present status and future. *Expert Rev. Vaccines* **2014**, *13*, 641−655.

(5) Romani, N.; et al. Targeting skin dendritic cells to improve intradermal vaccination. *Curr. Top. Microbiol. Immunol.* **2011**, *351*, 113−138.

(6) Kim, Y. C.; Park, J. H.; Prausnitz, M. R. Microneedles for drug and vaccine delivery. *Adv. Drug Delivery Rev.* **2012**, *64*, 1547−1568.

(7) Quinn, H. L.; Kearney, M. C.; Courtenay, A. J.; McCrudden, M. T.; Donnelly, R. F. The role of microneedles for drug and vaccine delivery. *Expert Opin. Drug Delivery* **2014**, *11*, 1769−1780.

DOI: 10.1021/acsbiomaterials.6b00414
ACS Biomater. Sci. Eng. 2017, 3, 195−205

(8) Indermun, S.; et al. Current advances in the fabrication of microneedles for transdermal delivery. *J. Controlled Release* **2014**, *185*, 130−138.
(9) Van Damme, P.; et al. Safety and efficacy of a novel microneedle device for dose sparing intradermal influenza vaccination in healthy adults. *Vaccine* **2009**, *27*, 454−459.
(10) DeMuth, P. C.; Moon, J. J.; Suh, H.; Hammond, P. T.; Irvine, D. J. Releasable layer-by-layer assembly of stabilized lipid nanocapsules on microneedles for enhanced transcutaneous vaccine delivery. *ACS Nano* **2012**, *6*, 8041−8051.
(11) Patel, S. R.; Lin, A. S.; Edelhauser, H. F.; Prausnitz, M. R. Suprachoroidal drug delivery to the back of the eye using hollow microneedles. *Pharm. Res.* **2011**, *28*, 166−176.
(12) Chu, R. S.; Targoni, O. S.; Krieg, A. M.; Lehmann, P. V.; Harding, C. V. CpG oligodeoxynucleotides act as adjuvants that switch on T helper 1 (Th1) immunity. *FASEB J.* **1998**, *12*, A612.
(13) Kim, Y. C.; Quan, F. S.; Compans, R. W.; Kang, S. M.; Prausnitz, M. R. Formulation and coating of microneedles with inactivated influenza virus to improve vaccine stability and immunogenicity. *J. Controlled Release* **2010**, *142*, 187−195.
(14) Sullivan, S. P.; et al. Dissolving polymer microneedle patches for influenza vaccination. *Nat. Med.* **2010**, *16*, 915−920.
(15) Pattani, A.; et al. Microneedle mediated intradermal delivery of adjuvanted recombinant HIV-1 CN54gp140 effectively primes mucosal boost inoculations. *J. Controlled Release* **2012**, *162*, 529−537.
(16) DeMuth, P. C.; et al. Polymer multilayer tattooing for enhanced DNA vaccination. *Nat. Mater.* **2013**, *12*, 367−376.
(17) DeMuth, P. C.; et al. Vaccine delivery with microneedle skin patches in nonhuman primates. *Nat. Biotechnol.* **2013**, *31*, 1082−1085.
(18) Kusamori, K.; et al. Development of a drug-coated microneedle array and its application for transdermal delivery of interferon alpha. *Biofabrication* **2016**, *8*, 015006.
(19) Gill, H. S.; Soderholm, J.; Prausnitz, M. R.; Sallberg, M. Cutaneous vaccination using microneedles coated with hepatitis C DNA vaccine. *Gene Ther.* **2010**, *17*, 811−814.
(20) van den Eertwegh, A. J.; et al. Combined immunotherapy with granulocyte-macrophage colony-stimulating factor-transduced allogeneic prostate cancer cells and ipilimumab in patients with metastatic castration-resistant prostate cancer: a phase 1 dose-escalation trial. *Lancet Oncol.* **2012**, *13*, 509−517.
(21) Eriksson, F.; Totterman, T.; Maltais, A. K.; Pisa, P.; Yachnin, J. DNA vaccine coding for the rhesus prostate specific antigen delivered by intradermal electroporation in patients with relapsed prostate cancer. *Vaccine* **2013**, *31*, 3843−3848.
(22) Bol, K. F.; et al. Prophylactic vaccines are potent activators of monocyte-derived dendritic cells and drive effective anti-tumor responses in melanoma patients at the cost of toxicity. *Cancer Immunol. Immunother.* **2016**, *65*, 327−339.
(23) Kumar, A.; et al. Microneedle-mediated transcutaneous immunization with plasmid DNA coated on cationic PLGA nanoparticles. *J. Controlled Release* **2012**, *163*, 230−239.
(24) Hu, Y.; et al. Microneedle-assisted dendritic cell-targeted nanoparticles for transcutaneous DNA immunization. *Polym. Chem.* **2015**, *6*, 373−379.
(25) Zaric, M.; et al. Skin dendritic cell targeting via microneedle arrays laden with antigen-encapsulated poly-D,L-lactide-co-glycolide nanoparticles induces efficient antitumor and antiviral immune responses. *ACS Nano* **2013**, *7*, 2042−2055.
(26) Zaric, M.; et al. Dissolving microneedle delivery of nanoparticle-encapsulated antigen elicits efficient cross-priming and Th1 immune responses by murine Langerhans cells. *J. Invest. Dermatol.* **2015**, *135*, 425−434.
(27) Lee, K.; Kim, J. D.; Lee, C. Y.; Her, S.; Jung, H. A high-capacity, hybrid electro-microneedle for in-situ cutaneous gene transfer. *Biomaterials* **2011**, *32*, 7705−7710.
(28) Chen, M. C.; Lin, Z. W.; Ling, M. H. Near-Infrared Light-Activatable Microneedle System for Treating Superficial Tumors by Combination of Chemotherapy and Photothermal Therapy. *ACS Nano* **2016**, *10*, 93−101.
(29) Wang, C.; Ye, Y.; Hochu, G. M.; Sadeghifar, H.; Gu, Z. Enhanced Cancer Immunotherapy by Microneedle Patch-Assisted Delivery of Anti-PD1 Antibody. *Nano Lett.* **2016**, *16*, 2334−2340.
(30) Saurer, E. M.; Flessner, R. M.; Sullivan, S. P.; Prausnitz, M. R.; Lynn, D. M. Layer-by-Layer Assembly of DNA- and Protein-Containing Films on Microneedles for Drug Delivery to the Skin. *Biomacromolecules* **2010**, *11*, 3136−3143.
(31) DeMuth, P. C.; Moon, J. J.; Suh, H.; Hammond, P. T.; Irvine, D. J. Releasable Layer-by-Layer Assembly of Stabilized Lipid Nanocapsules on Microneedles for Enhanced Transcutaneous Vaccine Delivery. *ACS Nano* **2012**, *6*, 8041−8051.
(32) DeMuth, P. C.; et al. Polymer multilayer tattooing for enhanced DNA vaccination. *Nat. Mater.* **2013**, *12*, 367−376.
(33) Kim, N. W.; et al. Polyplex-releasing microneedles for enhanced cutaneous delivery of DNA vaccine. *J. Controlled Release* **2014**, *179*, 11−17.
(34) Wang, T.; Wang, N. Biocompatible Mater Constructed Microneedle Arrays as a Novel Vaccine Adjuvant-Delivery System for Cutaneous and Mucosal Vaccination. *Curr. Pharm. Des.* **2015**, *21*, 5245−5255.
(35) Yan, Y.; Bjonmalm, M.; Caruso, F. Assembly of Layer-by-Layer Particles and Their Interactions with Biological Systems. *Chem. Mater.* **2014**, *26*, 452−460.
(36) Zhang, P.; Chiu, Y. C.; Tostanoski, L. H.; Jewell, C. M. Polyelectrolyte Multilayers Assembled Entirely from Immune Signals on Gold Nanoparticle Templates Promote Antigen-Specific T Cell Response. *ACS Nano* **2015**, *9*, 6465−6477.
(37) Chiu, Y. C.; Gammon, J. M.; Andorko, J. I.; Tostanoski, L. H.; Jewell, C. M. Modular Vaccine Design Using Carrier-Free Capsules Assembled from Polyionic Immune Signals. *ACS Biomater. Sci. Eng.* **2015**, *1*, 1200−1205.
(38) Chiu, Y. C.; Gammon, J. M.; Andorko, J. I.; Tostanoski, L. H.; Jewell, C. M. Assembly and Immunological Processing of Polyelectrolyte Multilayers Composed of Antigens and Adjuvants. *ACS Appl. Mater. Interfaces* **2016**, *8*, 18722.
(39) Xu, Z.; et al. Multifunctional nanoparticles co-delivering Trp2 peptide and CpG adjuvant induce potent cytotoxic T-lymphocyte response against melanoma and its lung metastasis. *J. Controlled Release* **2013**, *172*, 259−265.
(40) Shirota, H.; Klinman, D. M. Recent progress concerning CpG DNA and its use as a vaccine adjuvant. *Expert Rev. Vaccines* **2014**, *13*, 299−312.
(41) Mishra, B. B.; et al. Nitric oxide controls the immunopathology of tuberculosis by inhibiting NLRP3 inflammasome-dependent processing of IL-1beta. *Nat. Immunol.* **2013**, *14*, 52−60.
(42) Chiang, C. L. L.; Coukos, G.; Kandalaft, L. E. Whole Tumor Antigen Vaccines: Where Are We? *Vaccines* **2015**, *3*, 344−372.
(43) Wang, R. F.; Appella, E.; Kawakami, Y.; Kang, X. Q.; Rosenberg, S. A. Identification of TRP-2 as a human tumor antigen recognized by cytotoxic T lymphocytes. *J. Exp. Med.* **1996**, *184*, 2207−2216.
(44) Aurisicchio, L.; et al. Superior Immunologic and Therapeutic Efficacy of a Xenogeneic Genetic Cancer Vaccine Targeting Carcinoembryonic Human Antigen. *Hum. Gene Ther.* **2015**, *26*, 386−398.
(45) Shchukin, D. G.; Gorin, D. A.; Mohwald, H. Ultrasonically induced opening of polyelectrolyte microcontainers. *Langmuir* **2006**, *22*, 7400−7404.
(46) Lu, Z.; et al. Magnetic switch of permeability for polyelectrolyte microcapsules embedded with Co@Au nanoparticles. *Langmuir* **2005**, *21*, 2042−2050.
(47) Volodkin, D. V.; Madaboosi, N.; Blacklock, J.; Skirtach, A. G.; Mohwald, H. Surface-supported multilayers decorated with bio-active material aimed at light-triggered drug delivery. *Langmuir* **2009**, *25*, 14037−14043.
(48) van der Maaden, K.; et al. Ovalbumin-coated pH-sensitive microneedle arrays effectively induce ovalbumin-specific antibody and T-cell responses in mice. *Eur. J. Pharm. Biopharm.* **2014**, *88*, 310−315.

DOI: 10.1021/acsbiomaterials.6b00414
ACS Biomater. Sci. Eng. 2017, 3, 195−205

(49) Ariga, K.; Ji, Q. M.; Hill, J. P. Enzyme-Encapsulated Layer-by-Layer Assemblies: Current Status and Challenges Toward Ultimate Nanodevices. *Adv. Polym. Sci.* **2010**, *229*, 51−87.
(50) Jewell, C. M.; Lynn, D. M. Multilayered polyelectrolyte assemblies as platforms for the delivery of DNA and other nucleic acid-based therapeutics. *Adv. Drug Delivery Rev.* **2008**, *60*, 979−999.
(51) Shah, N. J.; et al. Adaptive growth factor delivery from a polyelectrolyte coating promotes synergistic bone tissue repair and reconstruction. *Proc. Natl. Acad. Sci. U. S. A.* **2014**, *111*, 12847−12852.
(52) Deshayes, S.; Morris, M. C.; Divita, G.; Heitz, F. Cell-penetrating peptides: tools for intracellular delivery of therapeutics. *Cell. Mol. Life Sci.* **2005**, *62*, 1839−1849.
(53) Copolovici, D. M.; Langel, K.; Eriste, E.; Langel, U. Cell-penetrating peptides: design, synthesis, and applications. *ACS Nano* **2014**, *8*, 1972−1994.
(54) Shrestha, N.; et al. Thiolation and Cell-Penetrating Peptide Surface Functionalization of Porous Silicon Nanoparticles for Oral Delivery of Insulin. *Adv. Funct. Mater.* **2016**, *26*, 3405−3416.
(55) Vazquez, E.; et al. Protein nanodisk assembling and intracellular trafficking powered by an arginine-rich (R9) peptide. *Nanomedicine* **2010**, *5*, 259−268.
(56) Jones, S. A. Directing transition from innate to acquired immunity: defining a role for IL-6. *J. Immunol.* **2005**, *175*, 3463−3468.
(57) Kayagaki, N.; et al. Noncanonical inflammasome activation by intracellular LPS independent of TLR4. *Science* **2013**, *341*, 1246−1249.
(58) Andorko, J. I.; Hess, K. L.; Jewell, C. M. Harnessing biomaterials to engineer the lymph node microenvironment for immunity or tolerance. *AAPS J.* **2015**, *17*, 323−338.
(59) Sharp, F. A.; et al. Uptake of particulate vaccine adjuvants by dendritic cells activates the NALP3 inflammasome. *Proc. Natl. Acad. Sci. U. S. A.* **2009**, *106*, 870−875.
(60) Demento, S. L.; et al. Inflammasome-activating nanoparticles as modular systems for optimizing vaccine efficacy. *Vaccine* **2009**, *27*, 3013−3021.
(61) Andorko, J. I.; Hess, K. L.; Pineault, K. G.; Jewell, C. M. Intrinsic immunogenicity of rapidly-degradable polymers evolves during degradation. *Acta Biomater.* **2016**, *32*, 24−34.
(62) Gammon, J. M.; Dold, N. M.; Jewell, C. M. Improving the clinical impact of biomaterials in cancer immunotherapy. *Oncotarget* **2016**, *7*, 15421−15443.
(63) Fearon, D. Combination immunotherapy for cancer. *J. Exp. Med.* **2016**, *213*, 1115.
(64) Khalil, D. N.; Smith, E. L.; Brentjens, R. J.; Wolchok, J. D. The future of cancer treatment: immunomodulation, CARs and combination immunotherapy. *Nat. Rev. Clin. Oncol.* **2016**, *13*, 394.

DOI: 10.1021/acsbiomaterials.6b00414
ACS Biomater. Sci. Eng. 2017, 3, 195−205